STM JOURNALS

Research & Reviews: Journal of
Physics

https://journals.stmjournals.com/rrjophy

ISSN: 2278-2265 (Online)
ISSN: 2347-9973 (Print)
Volume 14, Issue 2, 2025
May–August
DOI (Journal): 10.37591/RRJoPHY

Review RRJoPHY

Unraveling Mixed Ionic-Electronic Conduction in Lithium-Substituted Rubidium Tetra Titanates via Dielectric Spectroscopy and EPR Analysis

Shahanshah Haider Abdi[1], Dharmendra Kumar Dwivedee[2], Dharmendra Pal[3,*]

Abstract

Lithium-substituted Rubidium Tetra Titanates with varying concentrations of lithium carbonate (Li_2CO_3) — specifically 0.01, 0.05, and 0.1 molar percentages — were successfully synthesized using a conventional high-temperature solid-state reaction method. The resulting compounds follow the general chemical formula $Rb_{2-x}Li_xTi_4O_9$. X-ray diffraction (XRD) analysis confirmed that lithium ions were successfully incorporated into the crystal lattice without disrupting the fundamental layered structure of the host material. The crystal system remained monoclinic across all compositions (x = 0.01, 0.05, and 0.1), indicating structural stability even after lithium substitution. Further characterization of the samples was carried out using Electron Paramagnetic Resonance (EPR) spectroscopy and dielectric measurements in the high-temperature range of 373–798 K, within a frequency range of 100 kHz to 1 MHz. The EPR spectra provided evidence for the partial reduction of Ti^{4+} ions to Ti^{3+}, which suggests the presence of mixed valence states possibly contributing to the electrical conduction process. Dielectric and AC conductivity measurements revealed that lithium ions are primarily accommodated in the interlayer spaces traditionally occupied by rubidium ions, which subtly modifies the electrical properties. The temperature-dependent AC conductivity data, when plotted as ln(σT) versus 1000/T, revealed three distinct conduction regions. These regions are indicative of multiple conduction mechanisms operating over different temperature ranges. It was observed that these mechanisms are strongly dependent on the concentration of lithium, as well as the applied frequency and temperature. The conduction process appears to be dominated by thermally activated hopping at lower temperatures and grain boundary contributions at higher temperatures.

Keywords: Lithium substitution, $Rb_{2-x}Li_xTi_4O_9$, EPR spectroscopy, dielectric properties, AC conductivity

***Author for Correspondence**
Dharmendra Pal
E-mail: paldharmendra78@gmail.com

[1]Professor, Department of Physics, BBD Institute of Technology & Management, Lucknow, Uttar Pradesh, India
[2]Research Scholar, Department of Physics, Maharishi University of Information Technology, Lucknow, Uttar Pradesh, India
[3]Senior Faculty, Department of Physics, St. Fidelis College, Lucknow, Uttar Pradesh, India

Received Date: July 01, 2025
Accepted Date: August 09, 2025
Published Date: August 25, 2025

Citation: Shahanshah Haider Abdi, Dharmendra Kumar Dwivedee, Dharmendra Pal. Unraveling Mixed Ionic-Electronic Conduction in Lithium-Substituted Rubidium Tetra Titanates via Dielectric Spectroscopy and EPR Analysis. Research & Reviews: Journal of Physics. 2025; 14(2): 19–29p.

INTRODUCTION

A class of alkali metal titanates, generally represented by the formula $A_2O \cdot nTiO_2$ or $A_2Ti_nO_{2n+1}$ (where A is an alkali metal and $2 \leq n \leq 9$), is well known for forming layered or tunnel-type crystal structures depending on the value of *n* [1–5]. These titanates have attracted significant interest due to their high ion-exchange capabilities, which make them suitable host materials for incorporating organic guest molecules [6]. Earlier studies by Kikkawa et al. [7] explored the AC conductivity properties of compounds such as $Na_2Ti_3O_7$ and $K_2Ti_4O_9$, as well as their niobium-substituted derivatives. Our research group has also contributed to this area by investigating electron paramagnetic resonance (EPR) and DC conductivity in $Na_2Ti_3O_7$,

$K_2Ti_4O_9$, and their doped variants, including $K_{2-x}Rb_xTi_4O_9$ and iron/manganese-doped versions of the parent compounds [8–16]. More recently, Shripal et al. [17,18] have reported on dielectric spectroscopy of both pure and manganese-doped $Na_2Ti_3O_7$ and $K_2Ti_4O_9$ ceramics. The crystal structure of $Na_2Ti_3O_7$ is composed of $Ti_3O_7^{2-}$ layers aligned along the (100) plane. These layers are held together by sodium ions that occupy two distinct crystallographic sites. $Na_2Ti_3O_7$ crystallizes in a monoclinic system, with unit cell parameters: a = 0.9133 nm, b = 0.3806 nm, c = 0.8566 nm, and β = 101.57°, space group $P2_1/m$ [4]. Structural refinements have been detailed by O.V. Yakubovich and V.V. Kireev [19].

Machida et al. [20] investigated the pillaring behavior and photocatalytic properties of partially substituted layered titanates like $Na_2Ti_{3-x}M_xO_7$ and $K_2Ti_{4-x}M_xO_9$, where M = Mn, Fe, Co, Ni, or Cu. $Na_2Ti_3O_7$ powders with various grain sizes have been synthesized through solid-state reactions between Na_2CO_3 and TiO_2 [21]. The zigzag layered structure of $Na_2Ti_3O_7$ gives rise to three distinct dipole moments of 5.0, 5.8, and 6.2 Debye [22]. My previous research has also included EPR and electrical studies on Li-doped $Na_2Ti_3O_7$ ($Na_{1.9}Li_{0.1}Ti_3O_7$) and its copper-substituted counterparts [23]. In addition, I have reported on the mixed electronic–ionic conductivity of pure and manganese-doped Potassium Lithium Tetra Titanates ($K_{1.9}Li_{0.1}Ti_4O_9$) [24]. $K_2Ti_4O_9$ consists of layered networks of titanium-oxygen octahedra, with potassium ions residing in the interlayer space [25]. Like $Na_2Ti_3O_7$, it also has a monoclinic lattice, with cell parameters a = 1.8255 nm, b = 0.3790 nm, c = 1.2017 nm, and β = 106.43°.

The AC conductivity behavior of polycrystalline $Na_2Ti_3O_7$ and $K_2Ti_4O_9$, along with their niobium-substituted forms, was first studied by Kikkawa et al. [26]. These materials are also well known for their ion exchange reactions [27,28], and their crystal structures suggest potential for ionic conduction along the layers—making them excellent candidates for ion-exchange applications [28]. Inspired by these findings, in this paper, we report the EPR and dielectric spectroscopic studies of lithium-mixed Rubidium Tetra Titanates, synthesized with varying lithium content (molar percentage $0.0 \leq x \leq 0.1$). Our work aims to further understand the structural, electrical, and magnetic properties of these layered titanates and their potential functional applications.

EXPERIMENTAL PROCEDURES

In this study, lithium-substituted rubidium tetra titanate ceramics with the general formula $Rb_{2-x}Li_xTi_4O_9$ ($0.0 \leq x \leq 1.0$) were synthesized using a conventional high-temperature solid-state reaction technique. The structural, magnetic, and electrical properties of the synthesized samples were systematically investigated through X-ray diffraction (XRD), electron paramagnetic resonance (EPR), and AC conductivity measurements. The experimental procedures and characterization techniques employed are detailed in the following subsections.

Sample Preparation

Ceramic samples with the general formula $Rb_{2-x}Li_xTi_4O_9$ (where $0.0 \leq x \leq 1.0$) were prepared using the conventional high-temperature solid-state reaction method. Stoichiometric amounts of Rb_2CO_3 (99.9% pure, AR grade, Merck Germany), Li_2CO_3 (99.9% pure, AR grade, Merck Germany), and TiO_2 powder (99% pure, AR grade, Merck Germany) were thoroughly mixed and ground mechanically to obtain a fine, homogeneous powder. The powder mixture was initially calcined at 1100 K for 16 hours.After cooling to room temperature (RT), the calcined product was mixed with acetone and ground for an additional hour to ensure uniform particle size. This refined powder was subjected to a second heat treatment at 1100 K for 14 hours, followed by slow cooling to room temperature at a rate of 3.0 K per minute. The resulting powder was then compressed into pellets under a pressure of 15 MPa. These pellets, measuring approximately 10.25 mm in diameter and 1.25 mm in thickness, were wrapped in platinum foil and sintered once more at 1073 K for 14 hours, then cooled to room temperature at the same rate of 3.0 K per minute.

X-Ray Diffraction (XRD) Analysis

The crystal structure and phase composition of the sintered pellets were analyzed using an Iso-Debye Flex 2002 Rich-Seifert X-ray diffractometer, operated with Cu-Kα radiation at 30 kV and 20 mA.

Electron Paramagnetic Resonance (EPR) Analysis

EPR spectra were recorded using a Varian E-line Century Series E-109 spectrometer, operating in the X-band frequency range (~9.3 GHz). A 100 kHz field modulation was applied during the measurements. The magnetic field was precisely calibrated using a Varian E-500 digital NMR Gauss meter.

AC Conductivity Measurements

The sintered pellets were polished to obtain flat surfaces, which were then coated with high-purity silver paste and dried prior to electrical measurements. The samples were mounted in a holder and evacuated to 10^{-3} mbar before testing.

The loss tangent (tan δ) and parallel capacitance (Cp) were measured over varying frequencies and temperatures using an HP 4194A impedance analyzer. The bulk AC conductivity (σ) was calculated using the equation:

σ=G(tA)(i)σ = G \left(\frac{t}{A}\right) \tag{i}σ=G(At) (i)

Where:

- σ is the conductivity,
- G is the conductance,
- t is the thickness of the pellet,
- A is the cross-sectional area of the pellet.

RESULTS AND DISCUSSION

The XRD patterns of the synthesized $Rb_{2-x}Li_xTi_4O_9$ samples confirm the formation of a single-phase layered structure for all compositions within the range $0.0 \leq x \leq 0.1$. The monoclinic symmetry is retained across the lithium substitution series, indicating that lithium ions are successfully incorporated into the lattice without altering the fundamental crystal framework. EPR spectra reveal characteristic signals attributed to Ti^{3+} centers, suggesting a partial reduction of Ti^{4+} during the synthesis process. This indicates the presence of mixed valence states, which may contribute to enhanced electronic conduction. AC conductivity measurements further support this, showing thermally activated behavior over a wide temperature range. The conductivity increases with temperature, consistent with a hopping-type conduction mechanism. Additionally, a frequency-dependent dispersion in conductivity is observed, indicating the contribution of both grain and grain boundary effects. The data from ln(σT) vs. 1000/T plots exhibit three distinct conduction regions, each corresponding to different transport mechanisms influenced by lithium concentration and operating frequency. These findings suggest that lithium substitution plays a significant role in modifying the defect chemistry and enhancing the electrical performance of $Rb_2Ti_4O_9$-based ceramics.

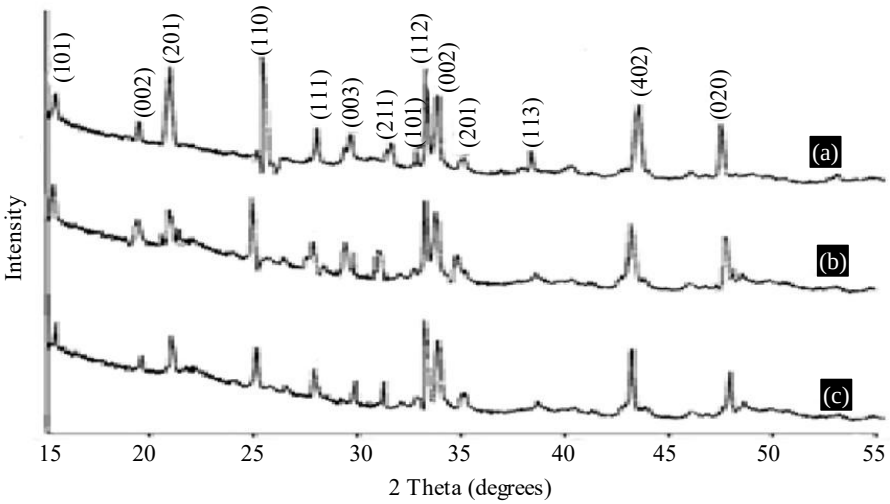

Figure 1. XRD of $Rb_{2-X}Li_XTi_4O_9$ with X= 0.01(a), 0.05(b) and 0.1(c).

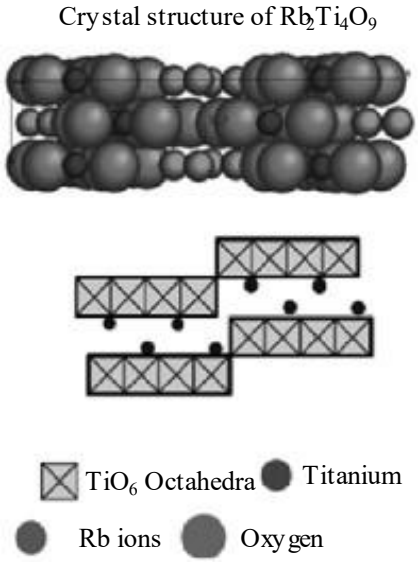

Figure 2. Schematic crystal structure of $Rb_2Ti_4O_9$.

XRD Analysis

The phase formation of sintered $Rb_{2-x}Li_xTi_4O_9$ ceramics, with x = 0.01, 0.05, and 0.1 mol% Li_2CO_3, was confirmed through X-ray diffraction (XRD) analysis, as shown in Figure 1. The diffraction patterns of all three lithium-substituted $Rb_2Ti_4O_9$ samples closely match those reported in previous literature [23, 29], indicating successful incorporation of lithium without the formation of secondary phases. The substitution of Li^+ ions (ionic radius ~0.076 nm) at Rb^+ sites (ionic radius ~0.102 nm) is structurally feasible due to the similarity in ionic sizes, albeit with a slight contraction of the lattice. The ceramic exhibits a layered structure composed of TiO_6 octahedra, with alkali ions located in the interlayer spaces. The resulting structure maintains a monoclinic symmetry, analogous to that of pure $Rb_2Ti_4O_9$, with reported lattice parameters: a = 1.8255 nm, b = 0.3790 nm, c = 1.2017 nm, and β = 106.43°.

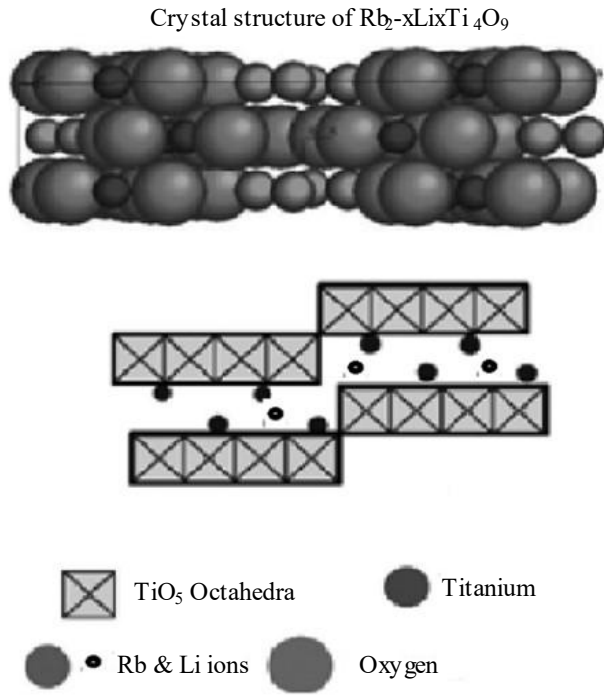

Figure 3. Schematic crystal structure of $Rb_{2-X}Li_XTi_4O_9$.

$Rb_2Ti_4O_9$ crystallizes in a monoclinic structure with the space group C2/m, forming a three-dimensional network. In this structure, Rb^+ ions are embedded within a framework of titanium and oxygen atoms. There are two distinct types of Rb^+ sites: in the first type, Rb^+ is surrounded by eight oxygen atoms, forming an 8-coordinate geometry with Rb–O bond lengths ranging from 2.86 to 3.23 Å. In the second site, Rb^+ exhibits a 6-coordinate geometry, bonded to six oxygen atoms with bond lengths between 2.81 and 3.16 Å.The Ti^{4+} ions occupy four inequivalent sites, each coordinated by six oxygen atoms, forming TiO_6 octahedra. These octahedra vary slightly in their bond distances and connect through both edge- and corner-sharing arrangements, creating a distorted lattice. The Ti–O bond lengths range from 1.74 to 2.37 Å, and some octahedra exhibit tilt angles of approximately 29° to 31°.There are also nine distinct oxygen (O^{2-}) sites, each showing different bonding geometries. These include linear, trigonal pyramidal, and more complex distorted configurations, involving connections to both Rb^+ and Ti^{4+} ions. The overall framework is made up of zig-zag chains of TiO_6 octahedra that extend along the b-axis, joined through shared corners and edges. The interlayer regions, where the Rb^+ ions reside, are relatively open and are located at two distinct vertical positions—Y = 1/4 and Y = 3/4—due to a lateral shift between adjacent layers. These spacious interlayer sites allow for possible substitution by smaller ions such as Li^+, which can modify the structure and electrical properties. The schematic representations of the crystal structures of both $Rb_2Ti_4O_9$ and its lithium-substituted form, $Rb_{2-x}Li_xTi_4O_9$, are illustrated in Figures 1-3.

which shows the presence of small Lithium ions with large Rubidium ions in the interlayer space.

EPR Spectra Analysis

The EPR spectra shown in Figure 2 of Li substituted $Rb_2Ti_4O_9$ [$Rb_{2-X}Li_XTi_4O_9$ with X= 0.01, 0.05 and 0.1] confirm the presence of Ti^{3+} ions, which result by the reduction of Ti^{4+} ions upon lithium. The g factor is 2.008 and falls in the range characteristic of d^1 ions in the distorted octahedral site. The absence of resolved hyperfine structure expected for the two titanium isotopes Ti (7.75% abundant, I = 5/2) and Ti (5.5% abundant, I=7/2) with the nuclear magnetic moment suggests that the unpaired spin is shared by several Ti nuclei. The substitution of Lithium ions in the interlayer space does not affect the crystal structure of $Rb_2Ti_4O_9$. This confirms the presence of small Lithium ions with large Potassium ions in the interlayer space. With the knowledge of about occupancy of Lithium ions in $Rb_2Ti_4O_9$ lattice, the ionic ac conductivity results can be discussed region wise Figure 4.

Ac Conductivity

Figure shows the variation of logarithmic ac conductivity (LnσT) as a function of reciprocal temperature (1000/T) for the compound $Rb_{1.99}Li_{0.01}Ti_4O_9$ at three different frequencies: 100 kHz, 500 kHz, and 1 MHz. The plots exhibit a typical thermally activated behavior, where conductivity increases with temperature, indicative of a semiconducting nature. At all three frequencies, the conductivity curves display non-linear regions across the temperature range, which suggests the presence of multiple conduction mechanisms. At lower temperatures (right side of the plot), the conductivity is low due to limited carrier mobility. As the temperature rises (moving left on the x-axis), the carriers gain sufficient thermal energy, leading to increased hopping and/or ionic movement within the lattice, thus enhancing conductivity. The higher the frequency, the lower the activation energy appears to be, as seen by the reduced slope of the curve. This suggests that electronic hopping conduction becomes more prominent at higher frequencies, while interlayer ionic conduction may dominate at lower frequencies and higher temperatures. The noticeable deviation in slope around the mid-temperature range might also indicate a transition from one dominant conduction mechanism to another, such as from localized electronic hopping to more delocalized or ionic transport, especially influenced by the presence of lithium ions at Rb+ sites. Overall, the figure supports the presence of a mixed conduction process in this Li-substituted titanate system, consistent with the layered structure and interlayer ion dynamics of the $Rb_2Ti_4O_9$ host lattice.

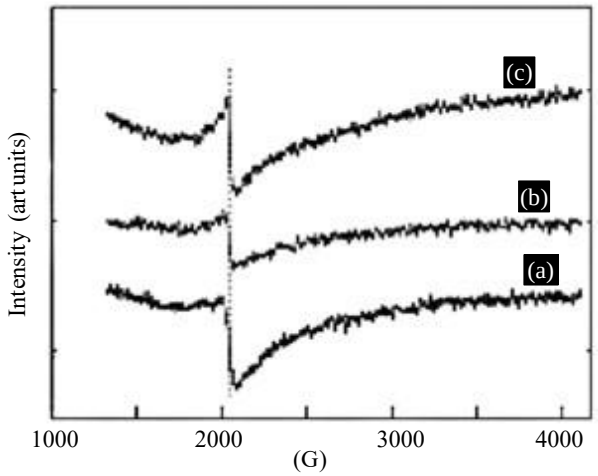

Figure 4. EPR spectra of lithium mixed rubidium tetra titanates $Rb_{2-X}Li_XTi_4O_9$ [X= 0.01(a), 0.05 (b) and 0.1(c)].

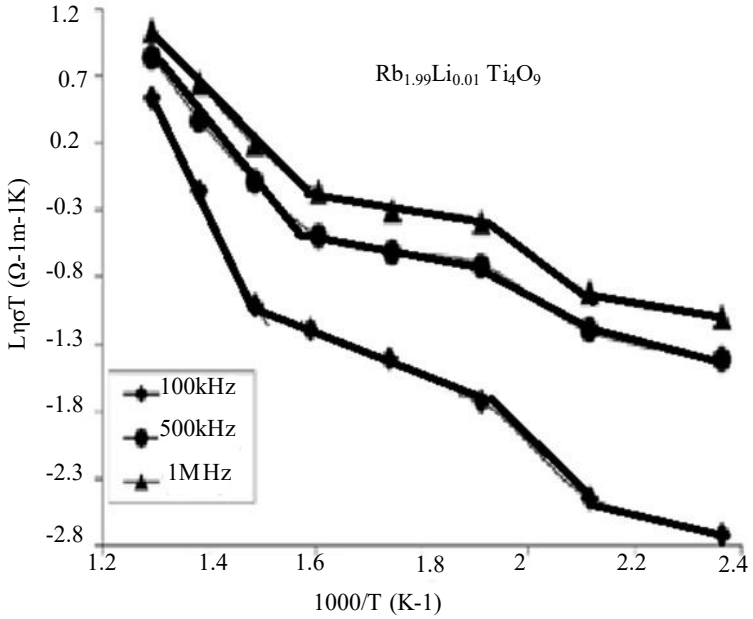

Figure 5. AC conductivity of $Rb_{1.99}Li_{0.01}Ti_4O_9$.

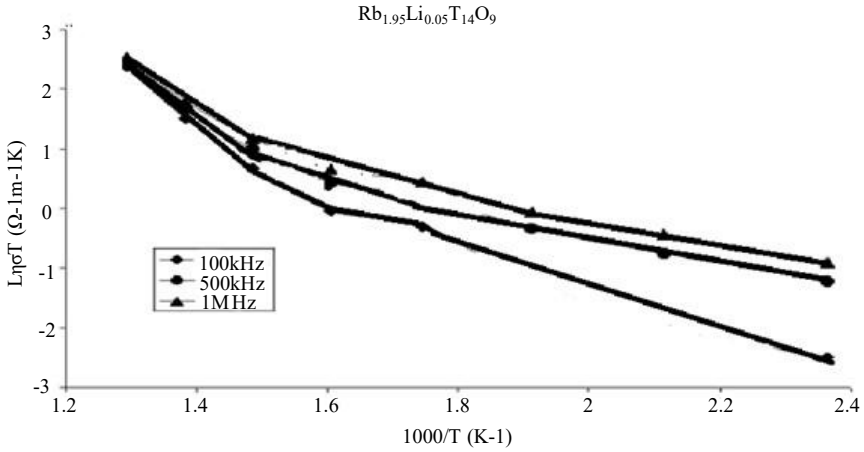

Figure 6. Temperature-dependent AC conductivity of $Rb_{1.95}Li_{0.05}Ti_4O_9$.

This figure illustrates the variation of logarithmic ac conductivity multiplied by temperature (LnσT) versus inverse temperature (1000/T) for $Rb_{1.95}Li_{0.05}Ti_4O_9$ at three frequencies: 100 kHz, 500 kHz, and 1 MHz. As seen in the plot, conductivity increases with increasing temperature, a typical signature of thermally activated transport. However, the behavior is clearly frequency-dependent, suggesting multiple overlapping conduction processes. The non-linearity in the mid-temperature range and the presence of distinct slopes in different temperature intervals indicate three conduction regions Figur 5-6:

1. *Low-temperature region (high 1000/T):* This region exhibits moderate temperature dependence, where electronic hopping conduction is dominant. The value of conductivity is slightly higher at increased frequencies, due to enhanced hopping probability among localized states.
2. *Intermediate region (mid-range 1000/T):* A noticeable inflection appears, possibly associated with a microstructural or phase-related transition. Lithium ions occupying Rb+ sites may alter the local bonding environment, leading to modified hopping pathways and additional ionic contributions to conduction.
3. *High-temperature region (low 1000/T):* A sharp increase in conductivity is observed, especially at 1 MHz, suggesting a transition to a conduction regime governed predominantly by interlayer ionic motion. Here, the increased thermal energy facilitates the movement of Li^+ and Rb^+ ions across the interlayer spaces in the lattice, contributing significantly to the overall conductivity.

Region I–Frequency-Dependent, Temperature-Independent Region

In this region, which extends up to 448 K for RLT-1, 473 K for RLT-2, and 498 K for RLT-3, the AC conductivity exhibits a clear dependence on frequency but shows minimal sensitivity to temperature changes. This behavior indicates that electronic hopping conduction is dominant here, occurring with a low activation energy, consistent with findings reported by Pal (2005). According to Joncher's model (1972), such frequency-dependent conductivity (proportional to ω^s, where $s < 1$) is typical for materials with low mobility and is attributed to a broad distribution of relaxation times, arising from varying hopping distances and energy barriers Figure 7-8.

The relatively higher AC conductivity compared to DC conductivity in this temperature range, as observed by Shripal et al., can be explained by coexisting electronic and interlayer ionic conduction. The peak observed around 473 K in the conductivity plot for RLT may result from Li^+ ions occupying interlayer positions, forming a stable Rb–Li–Ti configuration. This structural adjustment may decrease the availability of free electrons from $Ti_3O_7^{2-}$ units, thereby suppressing polaron hopping. In contrast, Cu-doped derivatives do not show this behavior, as ionic conduction through the interlayers appears to be absent. Prior studies support that electron hopping occurs in pure and Mn-doped titanates through loosely bound electrons jumping between adjacent Ti chains.

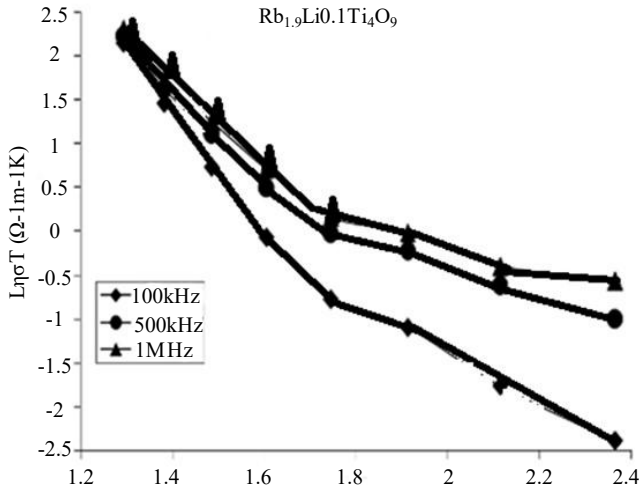

Figure 7. Temperature dependence ac conductivity plots for (a) RLT-1, (b) RLT-2 & (c) RLT-3 AC conductivity behavior and conduction mechanisms.

Anomalous Region

This transition region spans from 448–623 K for RLT-1, 473–548 K for RLT-2, and 498–598 K for RLT-3. A notable first peak at 523 K observed in all three compositions corresponds to a possible microstructural phase transition. A similar peak also appears in dielectric constant vs. temperature plots of Cu-doped derivatives. Additionally, the second peak at 598 K in the conductivity curve may be attributed to Li^+ substitution at Rb^+ sites, which could increase the number of mobile electrons capable of hopping along Ti-Ti chains, enhancing overall conductivity.

Region II – Temperature-Dependent, Frequency-Less-Dependent Region

This region shows stronger temperature dependence and reduced frequency sensitivity. It extends up to 648 K for RLT, and continues throughout the study range for RLT-1. For RLT-2 and RLT-3, this behavior spans 573–698 K and 623–698 K, respectively. The increased slope of conductivity plots suggests that interlayer ionic conduction becomes dominant, overtaking electronic hopping. According to Shripal et al. (1989), the presence of Rb–Li or Rb–Ti configurations introduces a relaxation-type behavior in the system. However, in RLT-3, due to the higher Li doping, a significant number of Mn ions occupy alkali interlayer sites, forming a compensatory structure that neutralizes the relaxation effects seen in lower-doped compositions. As a result, a relaxation peak near 500 K appears only at higher frequencies (above 100 kHz). Overall, conduction in this region can be described as a mixed mechanism, involving interlayer ionic transport, electron hopping, and alkali ion migration.

Region III – Strongly Temperature-Dependent, Frequency-Independent Region

Beyond 648 K for RLT and 698 K for RLT-2 and RLT-3, AC conductivity becomes almost entirely temperature-driven with little to no dependence on frequency. The steeper slope of the conductivity plots compared to earlier regions implies an enhanced conduction mechanism. It is proposed that Li^+ substitution at Rb^+ sites destabilizes some oxygen atoms from $Ti_3O_7^{2-}$ groups. These loosely bound oxygen atoms then begin participating in conduction as the dipoles formed with Rb^+/Li^+ break down. This marks the onset of what can be described as modified interlayer ionic conduction. The mechanism in this high-temperature range thus combines liberated oxygen ions, interlayer alkali ions, and potentially residual alkali ion hopping to facilitate conduction.

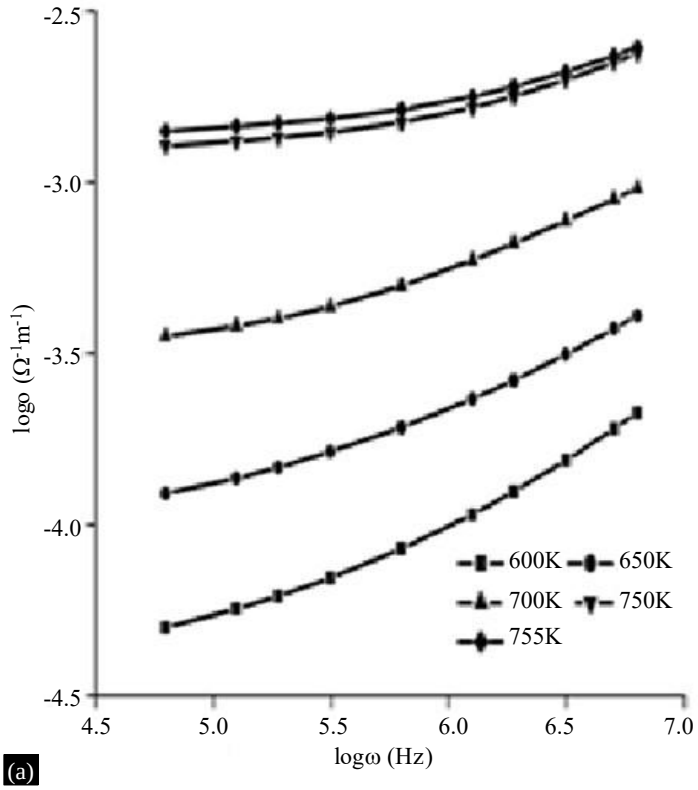

(a)

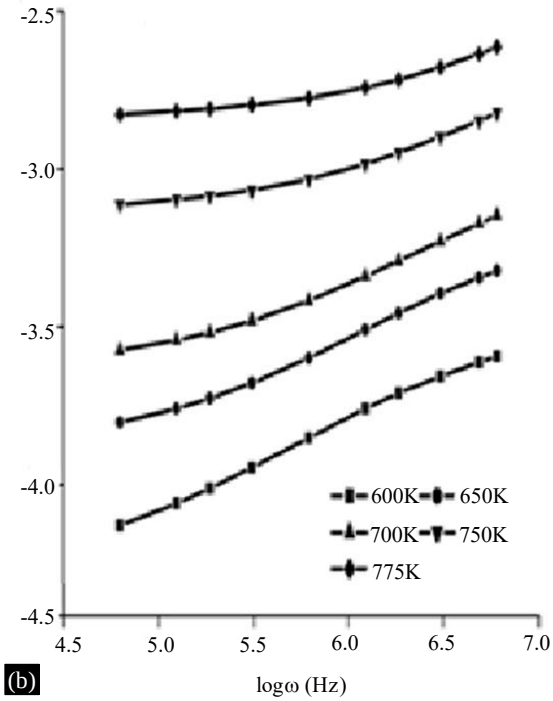

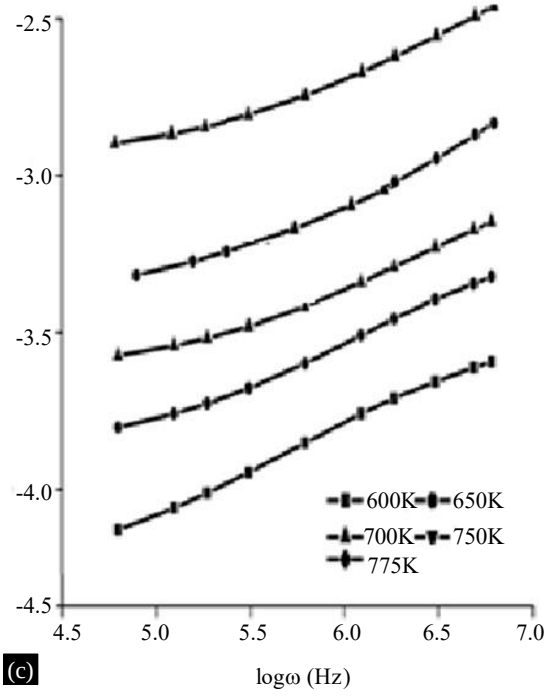

Figure 8. log(σ) versus frequency plots at different temperature (a) RLT-1, (b) RLT-2 and (c) RLT-3.

The conductivity log(σ) versus frequency log(ω) variations are given in Figure 8. From these plots, it can be seen that ac conductivity shows almost a linear variation with frequency at some fixed temperatures. For these samples, slopes are decreasing with the rise in temperature. As we know, every material has some free charges and under the applied low frequency, these charges can follow the eld and cause conduction currents. Polycrystalline materials have a short range order up to few molecular distances. Many research groups [31- 33] have interpreted such a behavior of conductivity due to the electronic hopping conduction and the ac conductivity shows almost a linear variation with frequency. Towards higher temperatures, we propose that alkali ion hopping conduction mechanism is responsible for frequency dependence of conductivity.

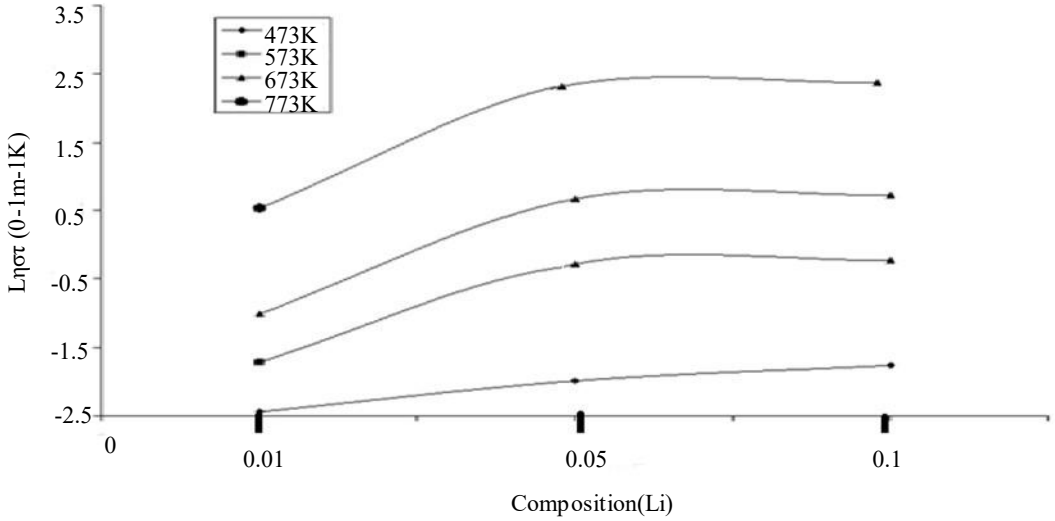

Figure 9. Effect of Li on ac conductivity (LnσT ($\Omega^{-1}m^{-1}K$) of Layered $Rb_2Ti_4O_9$.

Figure 9 shows the variation of LnσT vs. composition of Li (X). The conductivity increases as the lithium concentration increases. The electrical conductivity increases as the lithium concentration increases in all layered titanates, this is due to increase of ionic conduction in interlayer space.

CONCLUSIONS

The outcomes of the present investigations may be summarized as: For the first time-layered polycrystalline $Rb_{2-X}Li_XTi_4O_9$ (with X=0.01, 0.05 and 0.1) titanates have been synthesized and characterized through EPR and ac conductivity investigations.

The EPR spectra of Lithium mixed Rubidium Tetra Titanates confirm the partial reduction of Ti^{4+} ions to Ti^{3+}.

AC electrical conductivity studies show that the electronic hopping conduction exists in the entire temperature range of study and diminishes with rise in temperature.

a. In region I the proposed conduction mechanism is electronic hopping conduction or polaronic conduction.
b. The ionic conduction as 'Hindered interlayer ionic conduction' is proposed in region II.
c. The conduction mechanism in region III is associated interlayer ionic conduction with a part of electronic hopping conduction towards the lower temperature end of this region.
d. The dilation of zigzag interlayer space of $Rb_2Ti_4O_9$ (with X=0.01, 0.05 and 0.1) at the inclusion of Lithium ions has been identified in this work. Layered $Rb_{2-X}Li_XTi_4O_9$ (with X=0.01, 0.05 and 0.1) ceramics can be put in the class of mixed ionic-electronic materials.

REFERENCES

1. S. Anderson, A. D. Wadsley, Nature, 107, 499, (1960)
2. K. L. Berry, V. D. Aftandilian, W. W. Gilbert, H. P. Meibohm, H. S. Young, J. Inorg. Nucl. Chem. 14, 231, 1960
3. S. Anderson, A. D. Wadsley, Acta Chem. Scand, 15, 663 (1961)
4. S. Anderson, A. D. Wadsley, Acta Cryst. 14, 1245 (1961)
5. S. Anderson, A. D. Wadsley, Acta Cryst.15, 194,(1962)
6. H. Izawa, S. Kikkawa, M. Koizumi, J. Solid State Chem. 69, 336, (1987)
7. S. Kikkawa, F. Yasuda, and M. Koizumi, Mater. Res. Bull. 20, 1221(1985).
8. Shripal, S.D. Pandey, and Premchand, Solid State Commun. 69, 1203 (1989).
9. Shripal, Premchand and S.D. Pandey, J. Mater, Sci.: Mater. Electron. 2, 89 (1991).

10. Shripal, A.K. Mishra, and S.D. Pandey, and R.P. Tandon, Eur. J. Solid State Tnorg. Chem. 29. 229 (1992).
11. Shripal, R.P. Tandon, and S.D. Pandey, J. Phys. Chem. Solids 52, 1101(1991).
12. Dharmendra Pal, R.K. Pal, J.L. Pandey, S.H. Abdi, A.K. Agnihotri, J. Mater, Sci.: Mater. Electron. 21, 1181 (2010).
13. Dharmendra Pal and J.L. Pandey, Bull. Mater. Sci., 33(6), 691 (2010).
14. Dharmendra Pal, J.L. Pandey, Shripal, Journal of the Korean Chemical Society 53 (1), 42 (2009).
15. D. Pal, Premchand, R.P. Tandon, Shripal, Journal of the Korean Chemical Society 49 (6), 560 (2005).
16. D. Pal and Shripal, J. Mater. Sci: Mater Electron 18(4), 401 (2007)
17. Shripal, S. Badhwar, D. Maurya, J.Kumar, and R.P. Tandon, Advances in Condensed Matter Physics, edited by K.K. Raina (Allied New Delhi, 2005) p. 250.
18. Shripal, S. Badhwar, D. Maurya, J.Kumar, and R.P. Tandon, J. Mater, Sci.: Mater. Electron. 16, 495 (2005).
19. O. V. Yakubovich and V. V. Kireev, J. Crystallographic report, 48(1), 24, (2003)
20. Masato Machida, Xu. Wei Ma, Hideki Taniguchi, Jun-ichi Yabunaka, Tsuyoshi Kijima, J. Molecular catalysis A: chemical 155, 131 (2004)
21. Jaun Yang, Don Li, Xin Wang, Xujie Yang, Lude Lu, J. Mater. Sc. 38(13), 2907, (2003)
22. S. Ogura, K. Soto and Y. Inoue, Phys. Chem. Chem.. Phys. 2, 2449, (2002)
23. A. Verbaere and M. Tournoux, Bull. Soc. Chim, France, 4, 1237, (1973)
24. S. Kikkawa, F. Yasuda and M. Koizumi, Mater. Res. Bull. 20, 1221, (1985)
25. H. Izawa, S. Kikkawa, M. Koizumi, J. Phys. Chem., 86, 5023, (1982)
26. Y. Fujiki, F. Izumi, T. Ohsaka, M. Watanable, Yogya Kyo-Kailsh, 85, 475, (1977)
27. D. Pal, R. P. Tandon, Shripal, Indian Journal of Pure and Applied Physics, Vol. 44 (6), (2006) 435-439
28. A. Abragam and B. Bleaney, "Electron Paramagnetic Resonance of tranisition ions" (clarendon press, Oxford 1970) PP 455
29. D. Maurya, J. Kumar, Shripal, J. Phys. Chem. Solids 66, 1614 (2005).
30. S.D. Pandey, R.K. Sharma, Shripal, in: Proc. Fifth Asia Paci c Conf., Eds. S.P. Chia, K.S. Low, M. Oth- man, C.S. Wong, A.C. Chew, S.P. Moo, World Sci., Singapore 1992, p. 866.
31. G. Austin, N.F. Mott, Adv. Phys. 18, 41 (1969).
32. M. Pollack, Philos. Mag. 23, 519 (1971).
33. M. Bottger, V.V. Breyksin, Phys. Status Solidi 9, 79 (1976).

